nature photonics

Article

https://doi.org/10.1038/s41566-023-01267-0

Low-loss stable storage of 1.2 Å X-ray pulses in a 14 m Bragg cavity

Received: 10 January 2023

Accepted: 5 July 2023

Published online: 14 August 2023

Check for updates

Rachel Margraf[1,2], River Robles[1,2], Alex Halavanau[1], Jacek Kryzywinski[1], Kenan Li[1], James MacArthur[1], Taito Osaka[3], Anne Sakdinawat[1], Takahiro Sato[1], Yanwen Sun[1], Kenji Tamasaku[3,4], Zhirong Huang[1,2], Gabriel Marcus[1] ✉ & Diling Zhu[1] ✉

We present an experimental demonstration of a stable, low-loss, large X-ray cavity operating at 1.2 Å wavelength. The cavity consists of four separate high-reflectivity single crystal diamond Bragg mirrors arranged in a rectangular configuration with a round-trip distance of 14.2 m. Femtosecond X-ray pulses from an X-ray free-electron laser were coupled into the cavity via a transmission phase grating. We show that a stable mode can be maintained with the introduction of cavity focusing and measure round-trip efficiencies approaching 88%, or >96% when excluding grating and lens losses, close to the Bragg mirror theoretical performance limit. The direct observation of sustained stable X-ray circulation provides the most direct evidence to date that cavity-based X-ray free-electron lasers and other cavity-based hard X-ray systems are feasible.

In 1958, Schawlow and Townes[1] proposed an optical maser based on a gain medium introduced in a cavity with a single resonant mode[1]. Their work paved the way for modern laser oscillators, which have led to countless transformative applications in today's science and technology. Optical cavities, near ubiquitous among laser systems, typically play a large role in defining a laser's stable cavity modes and high temporal coherence. Unsurprisingly, the first free-electron lasers (FELs) were low-gain oscillators that utilized a cavity and operated at infrared, visible and ultraviolet wavelengths[2–4]. The oscillator concept was initially considered the most straightforward to scale towards shorter wavelengths[5,6], and the first proposal to use Bragg reflectors to circulate X-ray radiation was made in 1984[7]. However, when X-ray FELs (XFELs) were first conceived, the technology for constructing a large cavity at Angstrom wavelength was considered out of reach. Therefore, all current XFELs have adopted the single-pass, high-gain design[8–10]. This results in relatively poor temporal coherence of the emitted field, owing to the fundamental stochastic nature of the electron bunch dynamics. Hard X-ray self-seeding has been applied to improve coherence but still suffers from pulse energy instability[11–16]. Hard X-ray pulses with the full spatial and temporal coherence and high stability demanded by many new X-ray laser experimental techniques have yet to be demonstrated at any XFEL facility.

Many cavity-based conceptual design proposals for FELs have been studied, all projecting many orders of magnitude improvement in brightness and stability. In 2006, Huang and Ruth[17] proposed using a high-gain FEL in a Bragg cavity to form an X-ray regenerative amplifier XFEL[17–19]. In 2008, Kim et al.[20] proposed using a low-gain FEL to construct an oscillator[20]. More recently, Halavanau et al.[21] proposed using the Bragg cavity for a population-inversion X-ray laser oscillator. Upcoming experiments at both the Linac Coherent Light Source and European XFEL will provide early tests of these concepts[22,23]. In almost all proposals, Bragg optics, in particular single crystal diamonds, have been adopted as cavity optics due to their potential high reflectivity and superior thermal mechanical properties. This has since been experimentally verified via technological breakthroughs in the growth of defect- and strain-free synthetic diamond crystals[24,25]. A natural next step is to experimentally verify the performance of a Bragg X-ray cavity suitable for a cavity-based XFEL (CBXFEL), which can not only select a single longitudinal mode for amplification but also provide substantial suppression for undesired modes.

In contrast to the typical tabletop-scale cavities of optical lasers, or the micrometre to centimetre scale of previously demonstrated Bragg X-ray cavities[5,6,26], an X-ray cavity for a CBXFEL will require a much larger physical dimension, often approaching hundreds of metres in

[1]SLAC National Accelerator Laboratory, Menlo Park, CA, USA. [2]Applied Physics Department, Stanford University, Stanford, CA, USA. [3]RIKEN SPring-8 Center, Kouto, Sayo, Japan. [4]Japan Synchrotron Radiation Research Institute, Kouto, Sayo, Japan. ✉e-mail: gmarcus@slac.stanford.edu; dlzhu@slac.stanford.edu

https://doi.org/10.1038/s41566-023-01267-0

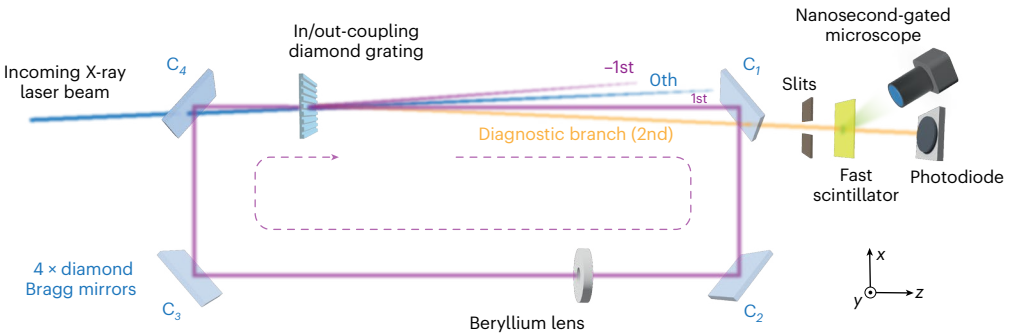

Fig. 1 | Experimental schematic of cavity optics and diagnostics. Four diamond Bragg mirrors are used as the main cavity optics. A portion of the incoming X-ray laser beam (blue, zeroth order) is injected into the cavity by a diamond transmission grating using its first-order diffraction (purple). The purple rectangle indicates the circulating beam trajectory inside the cavity once the correct photon energy has been chosen and the Bragg mirrors are aligned. A beryllium lens can be inserted into the beam path to stabilize the beam propagation over many round trips. The orange beam path indicates the first-order diffraction of the circulating beam (at second-order position with respect to the zeroth-order incoming beam) as it passes through the diamond grating each time. This beam was isolated and used for beam dynamics monitoring with a high-speed imager consisting of a fast scintillator and a nanosecond-gated microscope. The transmitted beam through the thin scintillator is measured by a downstream photodiode.

length. This footprint is driven by the physics of the gain media and gain process of an XFEL. Amplification requires interaction between X-ray pulses with a train of relativistic electron bunches through long undulators. The repetition rate of the electron source, dictating the cavity round-trip time, is governed by available high-brightness electron accelerators. For a modern superconducting linear accelerator with a megahertz-scale repetition rate, this sets the cavity length on the order of 100 m. The large cavity dimensions, in turn, demand very tight spatial and angular tolerances and requirements on the Bragg mirror system.

Here we report the performance of a 14.2 m round-trip length rectangular Bragg cavity operating at 1.261 Å as a critical demonstration towards realizing a full-scale CBXFEL. We show excellent short- and long-term cavity alignment and stability by the observation of nearly 60 single pulse X-ray round trips over a 2.8 μs time span, with minimal performance degradation over a period of 1 h. We investigate transverse cavity dynamics and the effects of intracavity focusing and show that cavity losses are close to theoretical values. The performance achieved by this X-ray cavity prototype, when compared with tolerance studies for CBXFEL systems[19], offers the most definitive demonstration to date that the realization of an operating cavity-based X-ray laser is technically feasible.

To utilize existing X-ray user infrastructure, we designed a 14.2 m cavity to fit within the footprint of the X-ray Pump-Probe endstation at the Linac Coherent Light Source[27]. A rectangular geometry was chosen for our test in the context of the CBXFEL project[22], where such a geometry provides more room for focusing and diagnostic elements in the return line than a backscattering geometry does[23]. This geometry also allows natural extension to larger lengths (hundreds of metres) without expanding laterally compared to a bow-tie cavity[18,21]. The operation wavelength was chosen at 1.261 Å (photon energy 9.831 keV) to enable high-efficiency Bragg reflection of diamond (400) at 45.000°. The X-ray Pump-Probe instrument monochromatized the input X-ray beam to a 0.6 eV bandwidth[28], and the beam divergence is approximately 3 μrad full width at half maximum when wavefront distortion from the monochromator is considered in addition to the natural FEL divergence[29]. Figure 1 shows the overall optical layout of the cavity. The X-ray beam enters the cavity by first transmitting through the diamond crystal C_4 and then through a transmission phase grating with a 1 μm period and 1.4% first-order diffraction efficiency[30]. The first diffraction order, which is deflected 126 μrad by the grating, is chosen as the in-coupled beam. It is reflected by the first Bragg mirror (C_1) at an exact 45.000° incidence angle. Other grating diffraction orders are outside the angular acceptance window of C_1 and therefore transmit downstream. The first order reflected off C_1, with its bandwidth reduced to ~100 meV by the spectral acceptance of C_1, is then reflected sequentially through C_2, C_3 and C_4 along the rectangular trajectory and arrives at the transmission grating again. This time, the directly transmitted zeroth order, with 93.4% efficiency (considering both absorption loss and diffraction loss), through the grating is chosen and carefully aligned to be colinear with the first-order diffraction from the incoming beam. This enables the beam to be reflected by C_1 again and subsequently recirculate in the cavity. A beryllium refractive lens[31] with a 71 m focal length (chosen as the strongest available focusing without increasing the beam divergence beyond the angular acceptance of the Bragg reflections) is inserted to further stabilize optical modes in the cavity. The recirculated beam path is enclosed by two vacuum chambers connected with beam transport tubes to eliminate air absorption losses; thus, the entire cavity is enclosed in vacuum. The first-order diffraction from the first round-trip return beam, as well as the later round trips, is separated in space and angle from the on-axis cavity recirculating beam after ~7 m of propagation distance. Other unwanted diffraction orders are filtered out with X-ray slits before a selected beam sample exits the cavity vacuum system through a Kapton window. A nanosecond-gated X-ray profile monitor is used to record the average beam position and profile after each round trip, while simultaneously the X-rays transmitting through the thin scintillator screen are collected by a fast photodiode that records each sample 'train' of the recirculating X-ray pulses. This allows for detailed dynamical measurements of the stored X-ray beam pulse property evolution over many passes.

Details of the cavity-loss mechanisms are critical in determining both the lasing threshold and the lasing performance characteristics in all CBXFELs. The overall round-trip loss, in combination with XFEL gain, determines how many round trips the system requires to reach saturation, as well as saturated output level. We evaluate the observed cavity round-trip losses by fitting a waveform to each peak in the averaged photodiode traces and comparing the amplitudes of all neighbouring peaks. Figure 2a,b shows these measurements after cavity alignment is optimized. In early passes, the trapped radiation undergoes spectral-angular filtering from the Bragg reflection process and incurs higher losses due to deviation from ideal alignment and cavity mode matching. We observe the per-round-trip efficiency grow quickly from 6% to >80%, as the fraction of matched cavity mode dominates the recirculating photon flux. This process reaches a quasi-steady state with round-trip efficiency asymptotically approaching ~88%. In this regime, if one excludes the measured 6.6% loss from the in/out-coupling grating

https://doi.org/10.1038/s41566-023-01267-0

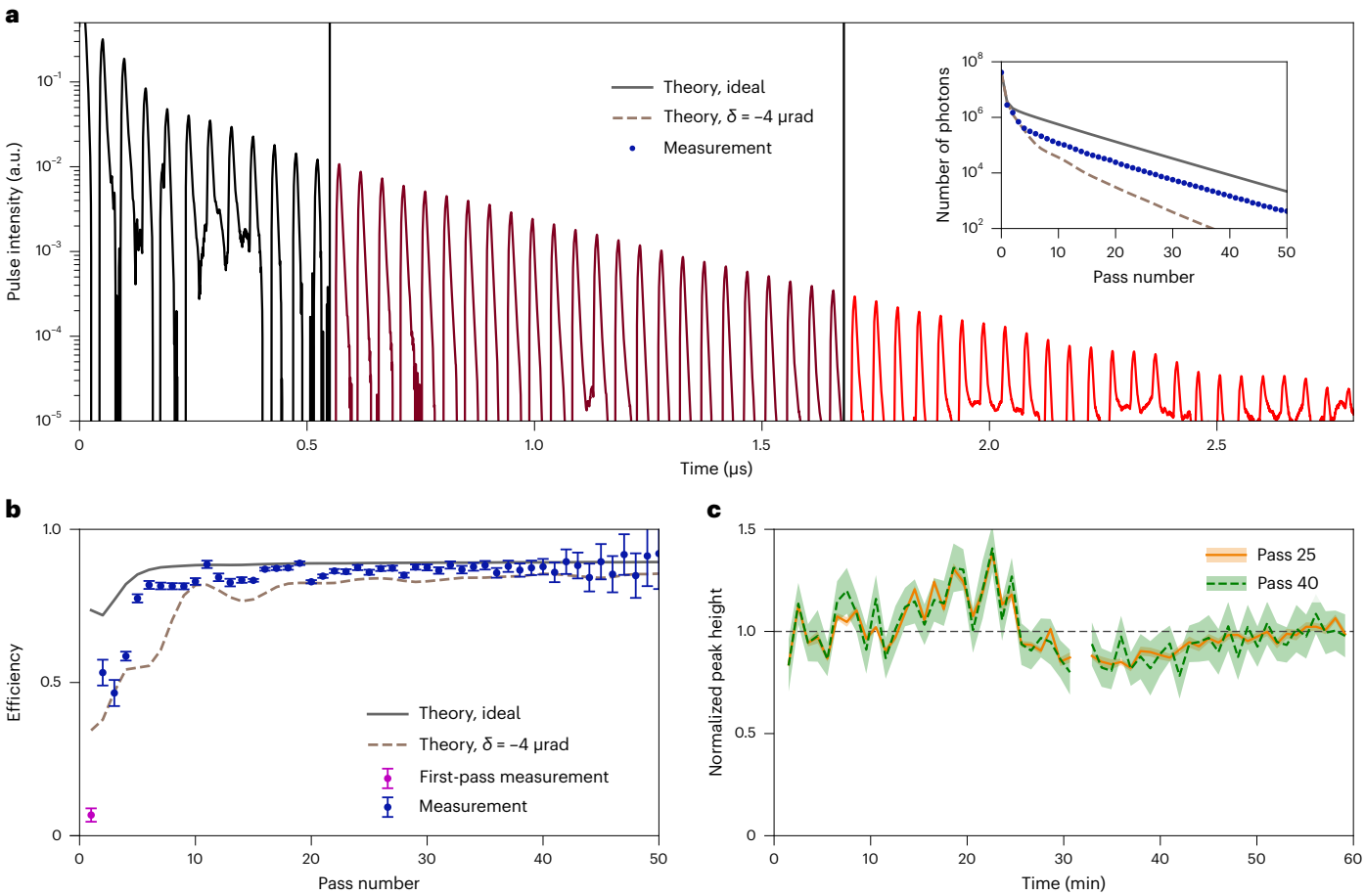

Fig. 2 | Cavity ring-down measurement with intracavity focusing (f = 71 m). **a**, Averaged ring-down measurements. Fifty-nine total round trips are shown within the 2.8 μs measurement window. Each region is averaged diode signal in arbitrary units (a.u.) after rejecting shots displaying detector saturation in passes 1–2 (black), passes 13–14 (maroon) and passes 34–35 (red). The inset shows an estimate of the average number of photons remaining in the cavity after each round trip. **b**, Cavity round-trip efficiency. Accompanying theory curves represent a numerical model assuming perfect alignment and a 4 μrad angular error in the input X-ray beam. The large energy bandwidth of the incident beam causes the first-pass efficiency to fall below the model, which assumes a narrow-bandwidth incident beam. Error bars represent systematic errors due to electronic noise, described in Supplementary Discussion Section 2. **c**, Average pulse intensity (normalized to average peak height and incoming pulse intensity downstream of the X-ray Pump-Probe monochromator) after round trips 25 and 40 over a 1 h period. Shaded regions represent systematic errors due to electronic noise, described in Supplementary Discussion Section 2.

for the zeroth order, and an estimate of 2% absorption loss from the lens, the matched mode has a round-trip efficiency of >96%. This indicates reflectivity for each individual diamond Bragg reflection of >99%, matching theoretical calculation from dynamical diffraction theory[32]. The solid and dashed lines in Fig. 2b are numerical beam propagation modelling results (Supplementary Discussion Section 1), with the upper boundary representing the case of ideal initial alignment and the lower boundary representing a compounded 4 μrad misalignment of the in-coupled X-ray beam from the cavity optical axis in the dispersion plane. The near-perfect round-trip efficiency observed at later round trips indicates that the quality of the synthetic high-pressure-high-temperature type IIa diamonds (Sumitomo Electric) is sufficient for them to serve as Bragg mirrors for cavity-based XFELs. While the initial alignment error can lead to longer build-up time for an X-ray laser cavity, as long as losses are overcome by the XFEL gain process, eventually the matched cavity mode will be amplified and dominate via optical gain guiding mechanisms[18–21,33]. The saturated XFEL performance after initial build-up will therefore be less affected by the early round-trip loss but largely determined by the later observed round-trip efficiency.

The inset in Fig. 2a shows the estimated number of photons in the cavity, using the efficiencies depicted in Fig. 2b. We estimate 65 nJ of pulse energy (60 μW mm^{-2} at 120 Hz) incident on C_1 before the first reflection, and expect negligible diamond heating in this cavity. For future cavity system implementation where 100 s of microjoule pulse energies (~1 kW mm^{-2} scale at 1 MHz) are anticipated[18], cooling of diamond optics will be required, as discussed in ref. 23.

The pulse energies at later round trips are extremely sensitive to the cavity alignment, serving as a direct indicator of the cavity's long-term stability. We found the cavity was able to maintain the average recirculating pulse energy at, for example, the 25th and the 40th round trips to within 30% of the initial value, as shown in Fig. 2c. This is comparable to the magnitude of impact from one minimal step Bragg angle adjustment, and indicates an overall angular alignment stability better than 400 nrad over the course of the 1 h measurement. This is also on the order of the ~350 nrad stability one would need to realize a high-gain, >100 m X-ray regenerative amplifier XFEL cavity scheme with gain guiding[19]. High-precision motion stages and active stabilization may be considered for improving the cavity stability further for low-gain, XFEL oscillator schemes.

The nanosecond-gated microscope provides direct measurement of the average beam position and size information after each round trip. The extracted beam profile images for sequential round

https://doi.org/10.1038/s41566-023-01267-0

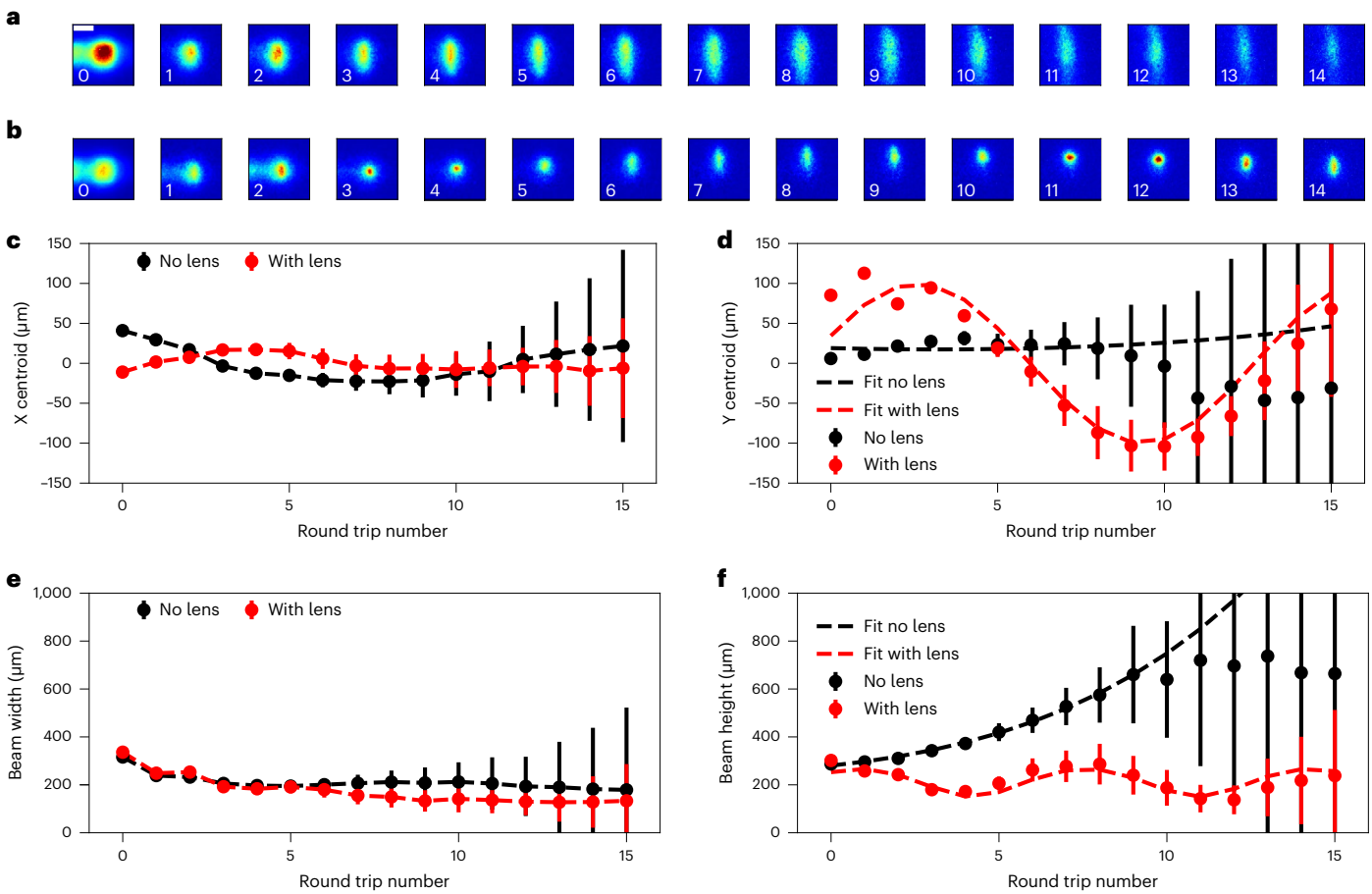

Fig. 3 | Transverse beam circulation dynamics. a,**b**, Beam spatial profile evolution in the X-ray cavity without (**a**) and with (**b**) intracavity focusing lens. The scale bar indicates 200 μm. **c**,**d**, Beam transverse positions after each round trip in the horizontal (**c**) and vertical (**d**) directions. **e**,**f**, Beam transverse sizes (full-width half-maximum) after each round trip in the horizontal (**e**) and vertical (**f**) directions. Vertical dynamics are accompanied by model fits based on linear optics tracking, while horizontal dynamics are accompanied by eye-guiding dashed lines. The centroid and widths reported are obtained from two-dimensional Gaussian fitting to those averaged images, with error bars indicating ± the reported uncertainty in that fitting parameter.

trips are shown in Fig. 3a,b for two different cavity configurations: only using the four Bragg mirrors (Fig. 3a) and with an $f = 71$ m focusing lens inserted (Fig. 3b). We find that in the case without intracavity focusing, while the beam position was optimized to remain relatively stable in both the horizontal and vertical directions (Fig. 3c,d), the vertical beam size quickly diverged (Fig. 3f). The increase in vertical beam size is faster than the natural divergence of the incoming FEL beam, indicating a compounded equivalent defocusing effect from the beamline monochromator and cavity diamond optics. In the horizontal direction, the beam size decreases from the ~350 μm initial value down to a size of 200 μm, the result of a slight focusing effect from the cavity crystals interacting with angular filtering of the Bragg reflections. When the intracavity focusing lens is inserted, a stable cavity is formed. We observe distinct beam size and position modulation in the vertical direction. Both beam size and trajectory oscillations in the nondispersive (vertical) plane can be modelled with ray optics (Fig. 3e,f and Supplementary Discussion Section 4), indicating effective intracavity focusing with $f = 93$ m. The observed beam centroid oscillations are analogous to particle accelerators (sometimes referred to as 'betatron oscillations' in accelerator physics)[34–36]. In the dispersion plane, due to dynamical diffraction, we again observed the effects of spectral-angular filtering, with the cavity mode size quickly reaching quasi-steady-state parameters. We note that in CBXFELs, electron beam transverse size and divergence can be adjusted to optimize the round-trip performance and alleviate the negative effects of the spectral-angular mismatch, by fine-tuning the magnetic transport lattice of the undulator.

In summary, we have experimentally demonstrated an operating large-scale X-ray cavity, based on four Bragg reflections, capable of storing X-rays for up to 2.8 μs. Intracavity focusing was shown to be effective in both selecting a well-defined recirculating mode and maintaining the cavity stability. An intracavity transmission grating was shown to be a simple and efficient way to in-couple and out-couple cavity radiation. This demonstration sets the foundation for cavities with gain—for example, a cavity-based XFEL, XFEL oscillator or X-ray laser oscillator. It also sets the stage for more complicated cavity designs with limited or extensive wavelength tunability, such as rectangular cavities with small-angle mirrors inserted in the return line or bow-tie cavities[18]. Other applications of this set-up include benchmarking of low-loss X-ray cavities for future light sources based on storage rings with cavity-based FEL oscillators[37], gamma–gamma scattering[38] imaging and quantum optics experiments[39], where a high coherence and a high repetition rate are required.

Online content

Any methods, additional references, Nature Portfolio reporting summaries, source data, extended data, supplementary information, acknowledgements, peer review information, details of author contributions and competing interests, and statements of data and code availability are available at https://doi.org/10.1038/s41566-023-01267-0.

References

1. Schawlow, A. L. & Townes, C. H. Infrared and optical masers. *Phys. Rev.* **112**, 1940–1949 (1958).
2. Madey, J. M. J. Stimulated emission of bremsstrahlung in a periodic magnetic field. *J. Appl. Phys.* **42**, 1906–1913 (1971).
3. Deacon, D. A. G. et al. First operation of a free-electron laser. *Phys. Rev. Lett.* **38**, 892–894 (1977).
4. Litvinenko, V., Burnham, B., Madey, J. & Wu, Y. Dynamics of the Duke storage ring UV FEL. *Nucl. Instrum.* **358**, 369–373 (1995).
5. Liss, K.-D. et al. Storage of X-ray photons in a crystal resonator. *Nature* **404**, 371–373 (2000).
6. Shvyd'ko, Y. V. et al. X-ray interferometry with microelectronvolt resolution. *Phys. Rev. Lett.* **90**, 013904 1–4 (2003).
7. Colella, R. & Luccio, A. Proposal for a free electron laser in the X-ray region. *Opt. Commun.* **50**, 41–44 (1984).
8. Kondratenko, A. M. & Saldin, E. L. Generation of coherent radiation by a relativistic electron beam in am undulator. *Part. Accel.* **10**, 207–216 (1980).
9. Bonifacio, R., Pellegrini, C. & Narducci, L. Collective instabilities and high-gain regime in a free electron laser. *Opt. Commun.* **50**, 373–378 (1984).
10. Kim, K., Huang, Z. & Lindberg, R. *Synchrotron Radiation and Free-Electron Lasers: Principles of Coherent X-Ray Generation* (Cambridge Univ. Press, 2017).
11. Amann, J. et al. Demonstration of self-seeding in a hard-X-ray free-electron laser. *Nat. Photon.* **6**, 693–698 (2012).
12. Inagaki, T. et al. Hard X-ray self-seeding set-up and results at SACLA. in *Proc. 36th International Free Electron Laser Conference, TUC01* (eds Chrin, J. et al.) 603–608 (JACoW, 2014).
13. Lutman, A. A. et al. Demonstration of single-crystal self-seeded two-color X-ray free-electron lasers. *Phys. Rev. Lett.* **113**, 254801 1–5 (2014).
14. Inoue, I. et al. Generation of narrow-band X-ray free-electron laser via reflection self-seeding. *Nat. Photon.* **13**, 319–322 (2019).
15. Nam, I. et al. High-brightness self-seeded X-ray free-electron laser covering the 3.5 keV to 14.6 keV range. *Nat. Photon.* **15**, 435–441 (2021).
16. Liu, S. et al. Cascaded hard X-ray self-seeded free-electron laser at MHz-repetition-rate. Preprint at *Research Square*, v1 https://doi.org/10.21203/rs.3.rs-2487501/v1 (2023).
17. Huang, Z. & Ruth, R. D. Fully coherent X-ray pulses from a regenerative-amplifier free-electron laser. *Phys. Rev. Lett.* **96**, 144801 1–4 (2006).
18. Marcus, G. et al. Refractive guide switching a regenerative amplifier free-electron laser for high peak and average power hard X-rays. *Phys. Rev. Lett.* **125**, 254801 1–6 (2020).
19. Marcus, G. et al. Regenerative amplification for a hard X-ray free-electron laser. in *Proc. of the Free Electron Laser Conference, TUP032 Vol. 39* (eds Decking, W. et al.) 118–121 (JACoW, 2019).
20. Kim, K.-J. et al. A proposal for an X-ray free-electron laser oscillator with an energy-recovery linac. *Phys. Rev. Lett.* **100**, 244802 1–4 (2008).
21. Halavanau, A. et al. Population inversion X-ray laser oscillator. *Proc. Natl Acad. Sci. USA* **117**, 15511–15516 (2020).
22. Marcus, G. et al. Cavity-based free-electron laser research and development: a joint Argonne National Laboratory and SLAC National Laboratory collaboration. in *Proc. of the Free Electron Laser Conference TUD04* (eds Decking, W. et al.) 282–287 (JACoW, 2019).
23. Rauer, P. et al. Cavity based X-ray free electron laser demonstrator at the European X-ray Free Electron Laser facility. *Phys. Rev. Accel. Beams* **26**, 020701 1–14 (2023).
24. Shvyd'ko, Y., Stoupin, S., Blank, V. & Terentyev, S. Near-100% Bragg reflectivity of X-rays. *Nat. Photon.* **5**, 539–542 (2011).
25. Sumiya, H., Harano, K. & Tamasaku, K. HPHT synthesis and crystalline quality of large high-quality (001) and (111) diamond crystals. *Diam. Relat. Mater.* **58**, 221–225 (2015).
26. Chang, S.-L. et al. Crystal cavity resonance for hard X-rays: a diffraction experiment. *Phys. Rev. B* **74**, 134111 1–7 (2006).
27. Chollet, M. et al. The X-ray Pump-Probe instrument at the Linac Coherent Light Source. *J. Synchrotron. Rad.* **22**, 503–507 (2015).
28. Zhu, D. et al. Performance of a beam-multiplexing diamond crystal monochromator at the Linac Coherent Light Source. *Rev. Sci. Instrum.* **85**, 063106 1–7 (2014).
29. Stoupin, S. et al. All-diamond optical assemblies for a beam-multiplexing X-ray monochromator at the Linac Coherent Light Source. *J. Appl. Crystallogr.* **47**, 1329–1336 (2014).
30. Li, K. et al. Wavefront preserving and high efficiency diamond grating beam splitter for X-ray free electron laser. *Opt. Express* **28**, 10939–10950 (2020).
31. Snigirev, A., Kohn, V., Snigireva, I. & Lengeler, B. A compound refractive lens for focusing high-energy X-rays. *Nature* **384**, 49–51 (1996).
32. Authier, A. *Dynamical Theory of X-ray Diffraction* (Oxford Univ. Press, 2001).
33. Scharlemann, E. T., Sessler, A. M. & Wurtele, J. S. Optical guiding in a free-electron laser. *Phys. Rev. Lett.* **54**, 1925–1928 (1985).
34. Blachman, N. M. & Courant, E. D. The dynamics of synchrotron with straight sections. *Rev. Sci. Instrum.* **20**, 596–601 (1949).
35. Qi, P. & Shvyd'ko, Y. Signatures of misalignment in X-ray cavities of cavity-based X-ray free-electron lasers. *Phys. Rev. Accel. Beams* **25**, 050701 1–20 (2022).
36. Tiwari, G. & Lindberg, R. R. Misalignment effects on the performance and stability of X-ray free-electron laser oscillator. *Phys. Rev. Accel. Beams* **25**, 090702 1–22 (2022).
37. Lindberg, R. R., Kim, K.-J., Cai, Y., Ding, Y. & Huang, Z. Transverse gradient undulators for a storage ring x-ray FEL oscillator. in *Proc. of the Free Electron Laser Conference THOBNO02* (eds Scholl, C. & Schaa, V.) 740–748 (JACoW, 2013).
38. Yamaji, T. et al. An experiment of X-ray photon-photon elastic scattering with a Laue-case beam collider. *Phys. Lett. B* **763**, 454–457 (2016).
39. Adams, B. W. et al. X-ray quantum optics. *J. Mod. Opt.* **60**, 2–21 (2013).

Methods

Cavity optics

The cavity Bragg mirrors were high-pressure-high-temperature type IIa single crystal diamond plates of thickness 270–600 µm, with C_4 being the thinnest. All the crystal surfaces were cut and polished along the (100) crystal planes, with strain-relief cuts added by laser micromachining to reduce strain from clamping[40]. The diamonds were characterized and selected based on rocking-curve imaging and surface asymmetry measurements to ensure a >1 × 1 mm^2 area with <0.2 µrad strain and <0.5° miscut. The crystal characterization process is described in more detail in refs. 41,42. The diamond transmission grating was fabricated on a chemical vapour deposition (CVD) polycrystalline diamond substrate with a thickness of 30 µm using reactive ion etching[30]. The grating period was 1 µm with an optical window size of 1 × 1 mm^2. The etch depth was chosen targeting a 1–2% first-order diffraction efficiency at 9.831 keV, optimized for a high zeroth-order diffraction efficiency and long cavity lifetime.

Cavity diagnostics

Initial crystal Bragg condition was established using large-area Canberra PIPS diodes positioned in the reflected beam path for each crystal. Time-resolved ring-down trace was measured using a high-speed photodiode (Optodiode AXUV20HS1) with a rise/fall time well below 10 ns when reverse biased. The signal was amplified using a broadband radiofrequency amplifier and recorded at 2 Gsps by an 8-bit digitizer (Agilent Acqiris DC282). An Andor iStar scientific Complementary Metal–Oxide–Semiconductor (sCMOS) camera with ultraviolet imaging optics was used to spatially and temporally resolve the X-ray beam profile after each round trip. A single crystal Ce:YAP scintillator of 30 µm thickness was used, taking advantage of its short fluorescence lifetime of ~25 ns at 370 nm. The combined time resolution of the imaging system was approximately 32 ns as shown in Supplementary Fig. 2. The sampled X-ray flux (10^4 photons per pulse) for later round trips was too low to allow single-shot imaging measurements. Multipulse exposure with synchronized electronic gating was used to obtain the beam profile measurements shown in Fig. 3. Fluorescence background subtraction from earlier round trips was removed according to the process shown in Supplementary Fig. 3.

Cavity alignment procedure

The initial diamond crystal orientation alignment was sequentially established by inserting large-area photodiodes after each crystal and maximizing the reflection. Once the first round-trip return was established, the diamond mirror Bragg angles were adjusted to guide the beam towards the zeroth round-trip beam position using the nanosecond-gated camera by iteratively steering the diamond Bragg mirrors. The exact photon energy was initially chosen by adjusting the upstream monochromator and changing the angles of $C_{1,2}$ to make the long sides of the rectangular beam path equal distance in the horizontal plane at the two ends of the cavity. Once the correct photon energy was identified, a waveform from the fast diode revealed the first few round trips. The final iterations involved microadjustments to the position and angle of the diamond Bragg mirrors to maximize the number of round trips seen in the ring-down waveform, and the pulse intensity of the last round trips. After optimal alignment was achieved, the beryllium lens (f = 71 m) was inserted to stabilize the beam trajectory inside the cavity.

Motorized rotation stages in the horizontal dispersion plane (Kohzu RA10A with 1:40 gear reduction and two-phase stepper motor) allow for an angular alignment precision of ~400 nrad with microstepping. In the vertical plane, three tilt stages (Kohzu SA07A) with a minimum step size of ~650 nrad were used. In addition, a piezo tilt stage (Attocube ECR5050hs) with a minimum step size of ~20 nrad was used for C_3. Each crystal's initial Bragg angle alignment based on a rocking-curve scan carried ~1 µrad uncertainty, contributing to lower pass-by-pass efficiency in the early round trips. However, this did not effect the steady-state cavity efficiency for the 'resonant' cavity mode as shown for later round trips in Fig. 2b.

Data availability

The data presented in the figures have been uploaded to Zenodo. Source data are provided with this paper. Additional raw data that support the findings of this study are available from the corresponding author upon reasonable request.

References

40. Pradhan, P. et al. Small Bragg-plane slope errors revealed in synthetic diamond crystals. *J. Synchrotron Rad.* **27**, 1553–1563 (2020).
41. Tamasaku, K., Ueda, T., Miwa, D. & Ishikawa, T. Goniometric and topographic characterization of synthetic IIa diamonds. *J. Phys. D: Appl. Phys.* **38**, A61–A66 (2005).
42. Halavanau, A. et al. Experimental setup for high-resolution characterization of crystal optics for coherent X-ray beam applications. *J. Appl. Crystallogr.* **56**, 155–159 (2023).

Acknowledgements

We are indebted to K.-J. Kim, Y. Shvyd'ko, R. Lindberg, D. Shu and H. Sumiya for insightful discussions. Diamond mirror characterization was performed at RIKEN SPring-8 (proposal numbers 20190013 and 20200085) and at the Stanford Synchrotron Radiation Light Source. Use of the Linac Coherent Light Source, SLAC National Accelerator Laboratory, was supported by the US Department of Energy, Office of Science, Office of Basic Energy Sciences under Contract No. DE-AC02-76SF00515. This research was also supported by the Department of Energy Laboratory Directed Research and Development programme at SLAC.

Author contributions

J.M., G.M., Z.H. and D.Z. conceived the experiment. R.M., R.R., A.H., K.L., T.O., A.S., T.S., Y.S., K.T., G.M. and D.Z. carried out the experiment. R.M., R.R., A.H., K.L., J.M., T.O., A.S., T.S. and K.T. prepared X-ray cavity optics. R.M., R.R., A.H., J.K., T.S., Y.S., G.M. and D.Z. performed the data analysis. R.M., R.R., A.H., G.M., Z.H. and D.Z. wrote the manuscript with input from all co-authors.

Competing interests

The authors declare no competing interests.

Additional information

Supplementary information The online version contains supplementary material available at https://doi.org/10.1038/s41566-023-01267-0.

Correspondence and requests for materials should be addressed to Gabriel Marcus or Diling Zhu.

Peer review information *Nature Photonics* thanks Enrico Allaria, Heung-Sik Kang, Jörg Rossbach, Timur Shaftan and the other, anonymous, reviewer(s) for their contribution to the peer review of this work.